Optimal and efficient shapes in acoustic boundary absorption

Frédéric Magoulès, Thi Phuong Kieu Nguyen, Pascal Omnes, Anna Rozanova-Pierrat

Optimal and efficient shapes in acoustic boundary absorption

Frédéric Magoulès* Thi Phuong Kieu Nguyen† Pascal Omnes‡

Anna Rozanova-Pierrat§

April 15, 2020

Abstract

In the aim to find the simplest and most efficient shape of a noise absorbing wall to dissipate the acoustical energy of a sound wave, we consider a frequency model described by the Helmholtz equation with a damping on the boundary. For the case of a regular boundary we provide the shape derivative of an objective function, chosen to describe the acoustical energy. Using the gradient method for the shape derivative, combined with the finite volume and level set methods, we find numerically the optimal shapes for a fixed frequency. We show the stability of the numerical algorithm and the non-uniqueness of the optimal shape, which can be explained by the non-uniqueness of the geometry providing the same spectral properties. We find numerically the most efficient shape in a range of frequencies, which contains different geometrical scales. Thus we show that if we simplify the obtained optimal shape, by deleting the smaller scales of the geometry, the new shape is efficient in the frequencies corresponding to its characteristic geometry scale length, but no more efficient in the higher frequencies.

Keywords: Shape optimization; Helmholtz equation; wave absorption; level set method; finite differences.

1 Introduction

In the framework of acoustical anti-noise walls, we consider the question of the simplest and most efficient shape of a noise absorbing wall to dissipate the energy of a sound wave. Knowing from [1] the existence of an optimal shape for a fixed frequency of a two-dimensional shape optimization problem for a Helmholtz equation with a damping on the boundary, we are interested in the same question numerically firstly for a fixed frequency and then for a frequency range.

The examples of existing anechoic chambers (electromagnetic or acoustic) show that the wave absorption works better with irregular absorbing walls. The first studies relating irregular geometry of a wall and absorption of a wave are performed numerically in [2]. Thus there is a question which is an optimal shape of a dissipative boundary to perform the maximal absorption of the energy of the wave? Naturally, the answere depends on the frequency and the wavelength of the way to absorb. In addition, if we think about noise of trains or cars, they cover a range of frequencies. Thus the same shape of an acoustic anti-noise wall should be efficient in this range of frequencies. And by the way, its shape cannot

*CentraleSupélec, Université Paris-Saclay, France.

†CentraleSupélec, Université Paris-Saclay, France.

‡DEN-Service de thermohydraulique et de mécanique des fluides (STMF), CEA, Université Paris-Saclay, France and Université Paris 13, LAGA, CNRS UMR 7539, Institut Galilée, France

§CentraleSupélec, Université Paris-Saclay, France (correspondence, anna.rozanova-pierrat@centralesupelec.fr).

be thought too complicated but corresponds to the industry constraint of its conception. With a developping of a $3D$ printing technics in the industry, we could however imagine more complicated shapes as initially developped for the demolding process[1].

We notice that the shape optimization of acoustical performances of the absorbing walls with the use of the shape derivative of the energy is never been done before. But there are a lot of studies of optimization of acoustic performances of non absorbing walls. For instance, Duhamel [3, 4] considers sound propagation in a two-dimensional vertical cut of a road wall and uses genetic algorithms to obtain optimal shapes (some of them are however not connected and thus could not be easily manufactured). The author also uses a branch and bound (combinatorial optimization) type linear programming in order to optimize the sensors' positions that allow an active noise control, following former work introduced by Lueg [5] in 1934. Abe et al. [6] consider a boundary elements based shape optimization of a non absorbing two-dimensional wall in the framework of a two-dimensional sound scattering problem for a fixed frequency (for the Helmholtz equation) using a topological derivative with the principle that a new shape or topology is obtained by nucleating small scattering bodies. Also for the Helmholtz equation for a fixed frequency, using the shape derivative of a functional representing the acoustical energy, Cao and Stanescu [7] consider a two-dimensional shape design problem for a non-absorbing part of the boundary to reduce the amount of noise radiated from aircraft turbofan engines. For the same problem, Farhadinia [8] developed a method based on measure theory, which does not require any information about gradients and the differentiability of the cost function.

On the other hand, for shape optimization problems there are theoretical results, reviewed in Refs. [9, 10], which rely on the topological derivatives of the cost functional to be minimized, with numerical application of the gradient method in both two and three dimensional cases (in the framework of solid mechanics). In particular, Achdou and Pironneau [11] considered the problem of optimization of a photocell, using a complex-valued Helmholtz problem with periodic boundary conditions with the aim to maximize the solar energy in a dissipative region. For acoustic waves in the two-dimensional case, optimization of the shape of an absorbing inclusion placed in a lossless acoustic medium was considered in Refs. [12, 13]. The considered model is the linear damped wave equation [14, 15]. Using the topology derivative approach, Münch et al. consider in [12, 13] the minimization of the acoustic energy of the solution of the damped wave equation at a given time $T > 0$ without any geometric restrictions and without the purpose of the design of an absorbent wall. See also [16] for the shape optimization of shell structure acoustics.

As in [1] we consider the frequency model described by the Helmholtz equation with a dissipation on a part of boundary given by a complex Robin boundary condition. It is the interface air-wall. In [1] it was shown that once the porous material of the wall is fixed, it is possible to find numerically the complex coefficient in the Robin boundary condition to obtain the same rate of energy dessipation by the boundary as for the two media model (air and porous wall) with the dissipation in volume presented by the linear damped wave equation. Thus, we use this approximation to calculate the complex coefficient in the Robin boundary condition for a porous material named ISOREL, frequently used in building insulation, and obtain for it all our numerical results, in particular in Section 5.

Thanks to the existence of an optimal shape realizing at least an infinum of the acoustical energy in a particular class of Lipschitz domains (see Definition 1), named admissible domains, for the Helmholtz problem with a complex Robin boundary condition, we develope here in the same framework the shape optimization algorithm. For the case of an admissible domain with a regular boundary we provide in Section 3 the shape derivative of an objective functional chosen to describe the acoustical energy.

Using the gradient descent method for the shape derivative, combined with the finite volume and level set methods introduced in Section 4, we find numerically optimal shapes for a fixed frequency in the two-dimensional case.

In Section 5, we show the stability of the numerical algorithm and the non-uniqueness of

[1] Fractal Wall, product of Colas Inc., French patent N0- 203404; U.S. patent 10"508,119.

the optimal shape, which can be explained by the non-uniqueness of the geometry providing the same spectral properties (see [17, 18, 19]). Numerically, we show that for efficiency in the energy absorption, the shape of the wall must be related with the half wavelength of the wave created by the source and thus it is not pertinent to add much smaller geometric variations, which finally confirms the possibility to create "not too complicated but most efficient" walls. At the same time, the multi-scale nature of the wall geometry is necessary for an efficient absorption in a large band of frequencies. We also find a most efficient shape of the wall on a large frequency interval and notice that the caracteristique geometric scale of the optimal shape is related with the This shape is multiscale, and we show that if we keep only the largest scale, the new shape has the same good dissipation properties as the optimal one in the low frequencies corresponding to the chosen scale length, but is no more efficient in higher frequencies, for which the deleted geometry scales where important.

To summarize, the rest of the paper is organized as follows. In Section 2 we introduce the acoustical model and the shape optimization framework from [1]. In Section 3 we find the shape derivative of the acoustical energy by the Lagrangian method and by a more rigorous method using the Eulerian derivative. In Section 4 we explaine the shape optimization algorithm based on a classical level set methods and the centered finite difference methode of solving the boundary problem for the Helmholtz equation. In Section 5 we present and explaine our numerical results firstly for the shape optimization for only one fixed frequency in Subsection 5.1 and then we develope an algorithm to find the most efficient shape in a large range of frequencies, given and discussed in Subsection 5.2.

2 Model and optimization framework

Let Ω be a connected bounded domain of $\mathbb{R}^2$ with a Lipschitz boundary $\partial\Omega$. We suppose that the boundary $\partial\Omega$ is divided into three parts $\partial\Omega = \Gamma_D \cup \Gamma_N \cup \Gamma$ and consider

$$\begin{cases} \triangle u + \omega^2 u = f(x), & x \in \Omega, \\ u = g(x) \quad \text{on } \Gamma_D, & \dfrac{\partial u}{\partial n} = 0 \quad \text{on } \Gamma_N, \quad \dfrac{\partial u}{\partial n} + \alpha(x)u = \mathrm{Tr}h(x) \quad \text{on } \Gamma, \end{cases} \tag{1}$$

where $\alpha(x)$ is a complex-valued regular function with a strictly positive real part ($\mathrm{Re}(\alpha) > 0$) and a strictly negative imaginary part ($\mathrm{Im}(\alpha) < 0$).

Remark 1. *This particular choice of the signs of the real and the imaginary parts of α are needed for the well-posedness properties [20] and the energy decay of the corresponding time-dependent problem. In addition, as the frequency $\omega > 0$ is supposed to be fixed, α can contain a dependence on ω, i.e., $\alpha \equiv \alpha(x, \omega)$.*

In this paper we work only with regular case, when the boundary of the domain Ω is not less than Lipschitz and we denote the Lebesgue measure on the boundary by σ. For the frequency model (1) on a domain with a regular boundary we introduce the Hilbert space

$$V(\Omega) = \{u \in H^1(\Omega) |\ u = 0 \text{ on } \Gamma_D\} \tag{2}$$

with the norm (equivalent to the usual norm $\|\cdot\|_{H^1(\Omega)}$)

$$\|u\|^2_{V(\Omega)} = \int_\Omega |\nabla u|^2 \mathrm{d}x + \int_\Gamma \mathrm{Re}(\alpha)|u|^2 \mathrm{d}\sigma,$$

and we refer to Theorem 2.1 [1] for the general well-posedness result. Here we are in particular interesting to the fact that if, for $m \in \mathbb{N}^*$, $\partial\Omega \in C^{m+2}$, $f \in H^m(\Omega)$ and $g \in H^{m+\frac{3}{2}}(\Gamma_D)$, then the unique solution u of the variational formulation for all $v \in V(\Omega)$

$$\int_\Omega \nabla u \cdot \nabla \bar{v} \mathrm{d}x - \omega^2 \int_\Omega u\bar{v} \mathrm{d}x + \int_\Gamma \alpha\, \mathrm{Tr}\, u\, \mathrm{Tr}\, \bar{v}\, \mathrm{d}\sigma = -\int_\Omega f\bar{v} \mathrm{d}x + \int_\Gamma \mathrm{Tr}\, h\, \mathrm{Tr}\, \bar{v}\, \mathrm{d}\sigma \tag{3}$$

belongs to $H^{m+2}(\Omega)$.

We consider the two dimensional shape design problem, which consists in optimizing the shape of Γ with the Robin dissipative condition in order to minimize the acoustic energy of system (1). The boundaries with the Neumann and Dirichlet conditions Γ_D and Γ_N are supposed to be fixed. We also define a fixed open set D with a Lipschitz boundary which contains all domains Ω. Actually, as only a part of the boundary (precisely Γ) changes its shape, we also impose that the changing part always lies inside of the closure of a fixed open set G with a Lipschitz boundary: $\Gamma \subset \overline{G}$. The set G forbids Γ to be too close to Γ_D, making the idea of an acoustical wall more realistic.

To introduce the class of admissible domains, on which we minimize as in [1] the acoustical energy of system (1), we define $\mathcal{L}ip$ as the class of all domains $\Omega \subset D$ for which

1. there exists a fixed $\varepsilon > 0$ such that all domains $\Omega \in \mathcal{L}ip$ satisfy the ε-cone property [21, 22]: for all $x \in \partial\Omega$, there exists $\xi_x \in \mathbb{R}^2$ with $\|\xi_x\| = 1$ such that for all $y \in \overline{\Omega} \cap B(x, \varepsilon)$
$$C(y, \xi_x, \varepsilon) = \{z \in \mathbb{R}^2 | (z - y, \xi_x) \geq \cos(\varepsilon)\|z - y\| \text{ and } 0 < \|z - y\| < \varepsilon\} \subset \Omega.$$
2. there exists a fixed $\hat{c} > 0$ such that for any $\Omega \in \mathcal{L}ip$ and for all $x \in \Gamma$ we have
$$\int_{\Gamma \cap B(x,r)} \mathrm{d}\sigma \leq \hat{c}r, \tag{4}$$
where $B(x, r)$ is the open Euclidean ball centered in x with radius r and λ is the usual one-dimensional Lebesgue measure on Γ.

The uniform ε-cone property implies, by Remark 2.4.8 [23, p. 55] and Theorem 2.4.7, that all boundaries of $\Omega \in \mathcal{L}ip$ are uniformly Lipschitz.

Let us notice that, by the boundedness of D containing all Ω, condition (4) implies that all Γ for $\Omega \in \mathcal{L}ip$ have uniform length: there exists $M > 0$ depending on the chosen $\hat{c} > 0$ such that for all $\Omega \in \mathcal{L}ip$ it holds $\mathrm{Vol}(\partial\Omega) = \int_{\partial\Omega} \mathrm{d}\sigma \leq M$.

The constant M (and hence initially $\hat{c}$) can be chosen arbitrary large but finite. We denote by $\Omega_0 \in \mathcal{L}ip$ and $\Gamma_0 \subset \overline{G}$ the "reference" domain and the "reference" boundary respectively (actually $\partial\Omega_0 = \Gamma_D \cup \Gamma_N \cup \Gamma_0$) corresponding to the initial shape before optimization.

Thus, the admissible class of domains can be defined as

Definition 1. *The set of domains*

$$U_{ad}(\Omega_0, \varepsilon, \hat{c}, G) = \{\Omega \in \mathcal{L}ip \,|\, \Gamma_D \cup \Gamma_N \subset \partial\Omega,\ \Gamma \subset \overline{G},\ M_0 \leq \int_\Gamma \mathrm{d}\sigma \leq M(\hat{c}),\ \int_\Omega \mathrm{d}x = \mathrm{Vol}(\Omega_0)\}, \tag{5}$$

is called the set of admissible domains.

Let us notice that we are interesting to fixe e $\hat{c}$ is sufficiently large in the aim to have a sufficiently large constant $M > 0$ in the sense that it is not less than $M_0 > 0$, which is the length of the straight line boundary. Moreover the case when M is equal to the length of the plane boundary M_0 is the trivial case when $U_{ad}(\Omega_0, \varepsilon, \hat{c}, G)$ contains only one unique domain with the plane boundary, which hence is trivially optimal. Therefore the problem becomes interesting for a sufficiently large M.

From the numerical point of view, the mesh of the finite differences shema give us only a finite number of admissible shapes. Thus the minimum of the energy is all times realized in the framework of the usual Lebesgue measure on Γ. Thus we can simplify the notations of [1] and to consider all time only the Lebesgue measure on Γ.

We define

$$J(\Omega, u(\Omega)) = A \int_\Omega |u(\Omega)|^2 \mathrm{d}x + B \int_\Omega |\nabla u(\Omega)|^2 \mathrm{d}x + C \int_\Gamma |u(\Omega)|^2 \mathrm{d}\sigma \tag{6}$$

In order to keep the volume constraint, instead of Eq. (6) we can also consider the objective function

$$J_1(\Omega, u(\Omega)) = A\int_\Omega |u(\Omega)|^2 \mathrm{d}x + B\int_\Omega |\nabla u(\Omega)|^2 \mathrm{d}x + C\int_\Gamma |u(\Omega)|^2 \mathrm{d}\sigma + \kappa(\mathrm{Vol}(\Omega) - \mathrm{Vol}(\Omega_0))^2, \tag{7}$$

where κ is some (large) positive constant penalizing the volume variation.

3 Shape derivative

We respectively denote by Ω_0 and Γ_0 the domain and the boundary of the initial shape before optimization. The optimization step modifies the initial shape of Ω_0 to $\Omega = (Id + \theta)\Omega_0$, according to the map $x \in \Omega_0 \mapsto (x + \theta(x)) \in \Omega$ and following the vector field $\theta \in W^{1,\infty}(\mathbb{R}^2, \mathbb{R}^2)$. Here Id is the identity map $x \in \mathbb{R}^2 \mapsto x \in \mathbb{R}^2$, $W^{1,\infty}(\mathbb{R}^2, \mathbb{R}^2)$ is the space of Lipschitz functions ϕ from $\mathbb{R}^2$ to $\mathbb{R}^2$, such that ϕ and $\nabla\phi$ are uniformly bounded in $\mathbb{R}^2$. Using the notations $|\cdot|_{\mathbb{R}^2}$ for the Euclidean norm in $\mathbb{R}^2$ and $|\cdot|_{\mathbb{R}^{2\times 2}}$ for the matrices Euclidean norm on $\mathbb{R}^2$, we define the norm on $W^{1,\infty}(\mathbb{R}^2, \mathbb{R}^2)$ by

$$\|\phi\|_{W^{1,\infty}(\mathbb{R}^2,\mathbb{R}^2)} = \sup_{x\in\mathbb{R}^2} \left(|\phi(x)|_{\mathbb{R}^2} + |\nabla\phi(x)|_{\mathbb{R}^{2\times 2}}\right).$$

Hence $\left(W^{1,\infty}(\mathbb{R}^2, \mathbb{R}^2), \|\cdot\|_{W^{1,\infty}(\mathbb{R}^2,\mathbb{R}^2)}\right)$ is a Banach space.

Let us start by introducing the definition of the shape derivative of a function.

Definition 2 (Shape derivative, [9])**.** *Let*

$$\mathcal{C}(\Omega_0) = \{\Omega \subset D \,|\, \exists\theta \in W^{1,\infty}(\mathbb{R}^2, \mathbb{R}^2), \|\theta\|_{W^{1,\infty}(\mathbb{R}^2,\mathbb{R}^2)} < 1, \Omega = (Id + \theta)\Omega_0\}.$$

The shape derivative of a function $K(\Omega) : \mathcal{C}(\Omega_0) \to \mathbb{R}$ at Ω_0 is defined as the Fréchet derivative in $W^{1,\infty}(\mathbb{R}^2, \mathbb{R}^2)$ at 0 of the function $\theta \mapsto K\left(Id + \theta\right)(\Omega_0)$, i.e.,

$$K\left(Id + \theta\right)(\Omega_0) = K(\Omega_0) + K'(\Omega_0)(\theta) + o(\theta) \quad \textit{with} \quad \lim_{\theta\to 0} \frac{\|o(\theta)\|_{L^\infty(\mathbb{R}^2)}}{\|\theta\|_{W^{1,\infty}(\mathbb{R}^2,\mathbb{R}^2)}} = 0,$$

where $K'(\Omega_0)$ is a continuous linear form on $W^{1,\infty}(\mathbb{R}^2, \mathbb{R}^2)$.

Let us introduce the Eulerian derivative (or shape derivative), denoted by U.

Definition 3 (Eulerian derivative)**.** *Assume that x belongs both to the initial domain Ω_0 and to the deformed domain $\Omega = (Id + \theta)(\Omega_0)$. A continuous linear form of $\theta \in W^{1,\infty}(\mathbb{R}^2, \mathbb{R}^2)$, denoted by $U(\theta, x)$, is called the Eulerian derivative, if it is defined by the expression:*

$$u\left((Id + \theta)(\Omega_0), x\right) = u(\Omega_0, x) + U(\theta, x) + o(\theta), \ \textit{with} \ \lim_{\theta\to 0} \frac{\|o(\theta)\|_{L^\infty(\mathbb{R}^2)}}{\|\theta\|_{W^{1,\infty}(\mathbb{R}^2,\mathbb{R}^2)}} = 0, \tag{8}$$

i.e., U is the directional derivative of u in the direction θ.

We recall an important result, which we use to compute the shape derivative of the objective functions J and J_1.

Lemma 1 (G. Allaire [9] Remark 6.29 p. 138)**.** *Let Ω_0 be an open bounded smooth domain in $\mathbb{R}^2$. Let $u(\Omega)$ be a function from $C(\Omega_0)$ to $L^1(\mathbb{R}^2)$. Then the function K_1 from $C(\Omega_0)$ to $\mathbb{R}$, defined by*

$$K_1(\Omega) = \int_\Omega u(\Omega)\mathrm{d}x,$$

is differentiable at Ω_0 *and for all* $\theta \in W^{1,\infty}(\mathbb{R}^2,\mathbb{R}^2)$*, we have*

$$K_1'(\Omega_0)(\theta) = \int_{\Omega_0} (U(\theta) + \operatorname{div}(u(\Omega_0)\theta))\,\mathrm{d}x.$$

Similarly, if $\hat{u}(\theta)$ *is derivable at* 0 *as function from* $C^1(\mathbb{R}^2,\mathbb{R}^2)$ *to* $L^1(\partial\Omega_0)$*, then*

$$K_2(\Omega) = \int_{\partial\Omega} u(\Omega)\mathrm{d}\sigma$$

is differentiable at Ω_0 *and, for all* $\theta \in C^1(\mathbb{R}^2,\mathbb{R}^2)$*, we have*

$$K_2'(\Omega_0)(\theta) = \int_{\partial\Omega_0} \left(U(\theta) + \theta\cdot n \left(\frac{\partial u(\Omega_0)}{\partial n} + Hu(\Omega_0) \right) \right) \mathrm{d}\sigma.$$

We prove the following theorem:

Theorem 1. *Let* Ω_0 *be a bounded domain in* $\mathbb{R}^2$ *with a connected boundary* $\partial\Omega_0 \in C^3$*, divided in three disjoint parts* $\partial\Omega_0 = \Gamma_0 \sqcup \Gamma_D \sqcup \Gamma_N$*. Let* $\Omega \in U_{ad}(\Omega_0,\varepsilon,\hat{c},G)$*, defined in* (5)*, and such that* $\partial\Omega = \Gamma \sqcup \Gamma_D \sqcup \Gamma_N$ *with* $\Gamma = (Id+\theta)\Gamma_0$ *(*$\theta \in W^{1,\infty}(\mathbb{R}^2,\mathbb{R}^2) \cap C^1(\mathbb{R}^2,\mathbb{R}^2)$ *and* $\|\theta\|_{W^{1,\infty}} < 1$*). Let* $u(\Omega_0) \in H^3(\Omega_0)$ *be the solution of problem* (1) *in* Ω_0 *with* $h = 0$*,* $g \in H^{\frac{5}{2}}(\Gamma_D)$ *and* $f \in H^1(\mathbb{R}^2)$ *(see Theorem 2.1 [1]). Then the shape derivative of the objective function* J_1 *defined by Eq.* (7)*, is given by*

$$J_1'(\Omega_0)(\theta) = \int_{\Gamma_0} (\theta\cdot n)(-\mathcal{V})\mathrm{d}\sigma, \tag{9}$$

where n *is the exterior normal vector on* Γ_0*, and the velocity* $-\mathcal{V}$ *is given by*

$$\begin{aligned} -\mathcal{V} = {} & \left(A|u|^2 + B|\nabla u|^2 + 2B|\alpha|^2|u|^2 - 4C\mathrm{Re}(\alpha)|u|^2 + CH|u|^2\right) \\ & + \mathrm{Re}\left(-\nabla u\cdot\nabla w + \omega^2 uw - fw - \alpha Huw + 2\alpha^2 uw\right) \\ & + 2\kappa\left(\mathrm{Vol}(\Omega) - \mathrm{Vol}(\Omega_0)\right) \end{aligned} \tag{10}$$

in which H *is the curvature of the boundary* Γ_0*, and* $w \in V(\Omega_0)$ *(*$V(\Omega_0)$ *is defined Eq.* (2)*) is the unique solution of the adjoint problem corresponding to* u*:*

$$\begin{cases} \triangle w + \omega^2 w = -2\left(A\bar{u}(\Omega_0) - B\triangle\bar{u}(\Omega_0)\right) & x \in \Omega_0, \\ w = 0 \quad on\ \Gamma_D, \quad \dfrac{\partial w}{\partial n} = 0 \quad on\ \Gamma_N, \\ \dfrac{\partial w}{\partial n} + \alpha w = -2B\bar{\alpha}\bar{u}(\Omega_0) + 2C\bar{u}(\Omega_0) \quad on\ \Gamma_0. \end{cases} \tag{11}$$

Proof. **Formal proof of Theorem 1 using the Lagrangian.** Since the data of the problem and the solution u are complex functions (except ω which is a positive constant), let us separate the imaginary and real parts, adopting the following notation: $u = u_R + iu_I$. Thus, the boundary value problem for the Helmholtz equation (1) takes the following form:

$$\triangle u_R + \omega^2 u_R = f_R(x) \quad x \in \Omega, \tag{12}$$

$$u_R = g_R(x) \quad \text{on } \Gamma_D, \quad \frac{\partial u_R}{\partial n} = 0 \quad \text{on } \Gamma_N, \quad \frac{\partial u_R}{\partial n} + \alpha_R u_R - \alpha_I u_I = 0 \quad \text{on } \Gamma,$$

$$\triangle u_I + \omega^2 u_I = f_I(x) \quad x \in \Omega, \tag{13}$$

$$u_I = g_I(x) \quad \text{on } \Gamma_D, \quad \frac{\partial u_I}{\partial n} = 0 \quad \text{on } \Gamma_N, \quad \frac{\partial u_I}{\partial n} + \alpha_I u_R + \alpha_R u_I = 0 \quad \text{on } \Gamma.$$

The objective function is considered as a function of the real and the complex parts of u:

$$\begin{aligned} J(\Omega,u_R,u_I) = {} & A\int_\Omega \left(|u_R|^2 + |u_I|^2\right)\mathrm{d}x + B\int_\Omega \left(|\nabla u_R|^2 + |\nabla u_I|^2\right)\mathrm{d}x \\ & + C\int_\Gamma \left(|u_R|^2 + |u_I|^2\right)\mathrm{d}\sigma. \end{aligned}$$

We write down the variational formulations for 12 and 13 and substract them to obtain for all $(w_R, w_I) \in V(\Omega) \times V(\Omega)$

$$
\begin{aligned}
&- \int_\Gamma \left((\alpha_R u_R - \alpha_I u_I)\, w_R - (\alpha_I u_R + \alpha_R u_I)\, w_I \right) \mathrm{d}\sigma \\
&+ \int_\Omega \left(\nabla u_I \nabla w_I - \nabla u_R \nabla w_R + \omega^2 \left(u_R w_R - u_I w_I \right) + f_I w_I - f_R w_R \right) \mathrm{d}x = 0. \qquad (14)
\end{aligned}
$$

We define (see [9] p. 152) the Lagrangian of the optimization problem as the sum of the functional J and the variational formulation (14)

$$
\begin{aligned}
&L(\Omega, u_R, u_I, w_R, w_I) = A \int_\Omega (|u_R|^2 + |u_I|^2) \mathrm{d}x \\
&+ B \int_\Omega (|\nabla u_R|^2 + |\nabla u_I|^2) \mathrm{d}x + C \int_\Gamma \left(|u_R|^2 + |u_I|^2 \right) \mathrm{d}\sigma \\
&+ \int_\Omega \left(\nabla u_I \nabla w_I - \nabla u_R \nabla w_R + \omega^2 \left(u_R w_R - u_I w_I \right) + f_I w_I - f_R w_R \right) \mathrm{d}x \\
&- \int_\Gamma \left((\alpha_R u_R - \alpha_I u_I)\, w_R - (\alpha_I u_R + \alpha_R u_I)\, w_I \right) \mathrm{d}\sigma, \qquad (15)
\end{aligned}
$$

where u_R, u_I, w_R and w_I are in $V(\Omega)$. The conjugate problem can be found from the system

$$
\left\langle \frac{\partial L}{\partial u_R}, \psi_R \right\rangle = 0, \quad \left\langle \frac{\partial L}{\partial u_I}, \psi_I \right\rangle = 0,
$$

with

$$
\begin{aligned}
\left\langle \frac{\partial L}{\partial u_R}, \psi_R \right\rangle = &\int_\Omega (2A u_R \psi_R + 2B \nabla u_R \nabla \psi_R - \nabla w_R \nabla \psi_R + \omega^2 w_R \psi_R) \mathrm{d}x \\
&- \int_\Gamma \left(\alpha_R w_R - \alpha_I w_I - 2C u_R \right) \psi_R \mathrm{d}\sigma
\end{aligned}
$$

and

$$
\begin{aligned}
\left\langle \frac{\partial L}{\partial u_I}, \psi_I \right\rangle = &\int_\Omega (2A u_I \psi_I + 2B \nabla u_I \nabla \psi_I + \nabla w_I \nabla \psi_I - \omega^2 w_I \psi_I) \mathrm{d}x \\
&+ \int_\Gamma \left(\alpha_I w_R + \alpha_R w_I + 2C u_I \right) \psi_I \mathrm{d}\sigma.
\end{aligned}
$$

This is the variational formulation of the following adjoint problem:

$$
\left\{
\begin{array}{l}
\triangle w_R + \omega^2 w_R = -2(A u_R(\Omega_0) - B \triangle u_R(\Omega_0)) \quad x \in \Omega_0, \\
w_R = 0 \quad \text{on } \Gamma_D, \quad \dfrac{\partial w_R}{\partial n} = 0 \quad \text{on } \Gamma_N, \\
\dfrac{\partial w_R}{\partial n} + \alpha_R w_R - \alpha_I w_I = -2B[\alpha_R u_R(\Omega_0) - \alpha_I u_I(\Omega_0)] + 2C u_R(\Omega_0) \quad \text{on } \Gamma_0, \\
\triangle w_I + \omega^2 w_I = 2(A u_I(\Omega_0) - B \triangle u_I(\Omega_0)) \quad x \in \Omega_0, \\
w_I = 0 \quad \text{on } \Gamma_D, \quad \dfrac{\partial w_I}{\partial n} = 0 \quad \text{on } \Gamma_N, \\
\dfrac{\partial w_I}{\partial n} + \alpha_I w_R + \alpha_R w_I = 2B(\alpha_R u_I(\Omega_0) + \alpha_I u_R(\Omega_0)) - 2C u_I(\Omega_0) \quad \text{on } \Gamma_0.
\end{array}
\right. \qquad (16)
$$

We notice that the adjoint problem (16) can be more compactly rewritten for the complex-valued functions $w \in V(\Omega_0)$ ($w = w_R + i w_I$), $u(\Omega_0)$ and α:

$$
\left\{
\begin{array}{l}
\triangle w + \omega^2 w = -2 \left(A \bar{u}(\Omega_0) - B \triangle \bar{u}(\Omega_0) \right) \; x \in \Omega_0, \\
w = 0 \quad \text{on } \Gamma_D, \quad \dfrac{\partial w}{\partial n} = 0 \quad \text{on } \Gamma_N, \\
\dfrac{\partial w}{\partial n} + \alpha w = -2B \bar{\alpha} \bar{u}(\Omega_0) + 2C \bar{u}(\Omega_0) \quad \text{on } \Gamma_0.
\end{array}
\right. \qquad (17)
$$

Hence, thanks to [9] Proposition 6.22 on p. 134 and Proposition 6.24 on p. 135, $J'(\Omega_0)(\theta)$ is given by the derivative of (15) over Ω:

$$\begin{aligned} J'(\Omega_0)(\theta) &= \frac{\partial L}{\partial \Omega}(\Omega_0, u_R, u_I, w_R, w_I)(\theta) \\ &= \int_{\Gamma_0} \theta \cdot n \left(A|u|^2 + B|\nabla u|^2 - 2C\mathrm{Re}(\alpha)|u|^2 + CH|u|^2 \right) \mathrm{d}\sigma \\ &+ \int_{\Gamma_0} \theta \cdot n \mathrm{Re}\left(-\nabla u \cdot \nabla w + \omega^2 uw - fw - \alpha H uw - \alpha \frac{\partial (uw)}{\partial n} \right) \mathrm{d}\sigma, \end{aligned} \tag{18}$$

where n is the outward normal on Γ_0 and H is the curvature of Γ_0. Using the boundary conditions and adding the volume constraint, we directly obtain (9) which concludes the proof.

Rigorous proof of Theorem 1. Since Γ_D does not move in our assumption, and thus, the value g does not have any influence on the shape derivative $J'(\Omega_0)$, in what follows, in the aim to simplify the notations, we take $g \equiv 0$ on Γ_D. Let us follow the proof of Theorem 6.38 pp. 145–146 of G. Allaire [9] (see also on p. 144 the proof of Corollary 6.36).

Thanks to 1, we find the shape derivative of J as

$$\begin{aligned} J'(\Omega_0)(\theta) &= \int_{\Omega_0} \mathrm{div}\left(\theta \left(A|u(\Omega_0)|^2 + B|\nabla u(\Omega_0)|^2 \right) \right) \mathrm{d}x \\ &+ C \int_{\Gamma_0} \theta \cdot n \left(\frac{\partial |u(\Omega_0)|^2}{\partial n} + H|u(\Omega_0)|^2 \right) \mathrm{d}\sigma + 2C \int_{\Gamma_0} \mathrm{Re}(\bar{u}(\Omega_0) U) \mathrm{d}\sigma \\ &+ \int_{\Omega_0} \left(2A\mathrm{Re}(\bar{u}(\Omega_0)U) + 2B\mathrm{Re}(\nabla \bar{u}(\Omega_0) \cdot \nabla U) \right) \mathrm{d}x \\ &= \int_{\Gamma_0} \theta \cdot n \left(A|u(\Omega_0)|^2 + B|\nabla u(\Omega_0)|^2 + C\frac{\partial |u(\Omega_0)|^2}{\partial n} + CH|u(\Omega_0)|^2 \right) \mathrm{d}\sigma \\ &+ \int_{\Omega_0} \mathrm{Re}\left(2A\bar{u}(\Omega_0)U + 2B\nabla \bar{u}(\Omega_0) \cdot \nabla U \right) \mathrm{d}x + 2C \int_{\Gamma_0} \mathrm{Re}(\bar{u}(\Omega_0)U) \mathrm{d}\sigma, \end{aligned} \tag{19}$$

where U is the Eulerian derivative. We need now to precise the real part of the variational formulation for the adjoint problem (see system (17)) taking $\overline{U}$ as the test function:

$$\begin{aligned} &\mathrm{Re}\left(\int_{\Omega_0} \nabla w \nabla U \mathrm{d}x - \omega^2 \int_{\Omega_0} wU \mathrm{d}x + \int_{\Gamma_0} \alpha w U \mathrm{d}\sigma \right) \\ &\qquad = \int_{\Omega_0} \mathrm{Re}\left(2A\bar{u}(\Omega_0)U + 2B\nabla \bar{u}(\Omega_0) \nabla U \right) \mathrm{d}x + 2C \int_{\Gamma_0} \mathrm{Re}(\bar{u}(\Omega_0)U) \mathrm{d}\sigma. \end{aligned} \tag{20}$$

We notice that in the right-hand side (as the source terms) of (20) we have all integrals from (19) involving U.

Thanks to the regularity of the boundary $\partial\Omega$, the elements of $H^1(\Omega)$ can be considered as the restrictions of the corresponding elements of $H^1(\mathbb{R}^2)$. Thus, we can reformulate the variational form (3) by "find $u(\Omega) \in V(\mathbb{R}^2)$, such that

$$\forall v \in V(\mathbb{R}^2) \quad - \int_{\Omega} \nabla u \cdot \nabla \bar{v} \mathrm{d}x + \omega^2 \int_{\Omega} u\bar{v} \mathrm{d}x - \int_{\Gamma} \alpha u \bar{v} \mathrm{d}\sigma = \int_{\Omega} f\bar{v} \mathrm{d}x."$$

We derive the last equality in Ω_0, using Lemma 1 and the facts, that $\theta = 0$ on Γ_D and Γ_N. Hence, we find that $u'(\Omega_0)(\theta) = U$, the Eulerian derivative of u, verifies

$$\begin{aligned} &\forall v \in V(\Omega_0) \quad \int_{\Omega_0} (-\nabla U \cdot \nabla \overline{v} + \omega^2 U \overline{v}) \mathrm{d}x - \int_{\Gamma_0} \alpha U \overline{v} \mathrm{d}\sigma \\ &= \int_{\Gamma_0} \theta \cdot n \left(\nabla u \cdot \nabla \overline{v} - \omega^2 u \overline{v} + f\overline{v} + \alpha H u \overline{v} + \alpha \frac{\partial (u\overline{v})}{\partial n} \right) \mathrm{d}\sigma. \end{aligned} \tag{21}$$

In particular (21) holds for $v = \overline{w}$, with w the weak solution of the adjoint problem (17). Hence, from (21) with $v = \overline{w}$ and from (20) we find

$$\int_{\Omega_0} \mathrm{Re}\left(2A\bar{u}(\Omega_0)U + 2B\nabla\bar{u}(\Omega_0)\nabla U\right)\mathrm{d}x + \int_{\Gamma_0} 2C\mathrm{Re}(\bar{u}(\Omega_0)U)\mathrm{d}\sigma$$
$$= \int_{\Gamma_0} \theta\cdot n\mathrm{Re}\left(-\nabla u(\Omega_0)\cdot\nabla w + \omega^2 u(\Omega_0)w - fw - \alpha H u(\Omega_0)w - \alpha\frac{\partial(u(\Omega_0)w)}{\partial n}\right)\mathrm{d}\sigma.$$

Finally, by inserting the above formula into (19) and using the following equality inferred from the Robin boundary conditions for u and w on Γ_0:

$$\alpha\nabla(uw)\cdot n = \alpha\left(w\nabla u\cdot n + u\nabla w\cdot n\right) = -2\alpha^2 uw - 2B|\alpha|^2|u|^2 + 2C\alpha|u|^2,$$

we obtain that

$$J'(\Omega_0)(\theta) = \int_{\Gamma_0} \theta\cdot n\left(A|u(\Omega_0)|^2 + B|\nabla u(\Omega_0)|^2 + 2B|\alpha|^2|u(\Omega_0)|^2\right.$$
$$\left.-4C\mathrm{Re}(\alpha)|u(\Omega_0)|^2 + CH|u(\Omega_0)|^2\right)\mathrm{d}\sigma$$
$$+\int_{\Gamma_0} \theta\cdot n\mathrm{Re}\left(-\nabla u(\Omega_0)\cdot\nabla w + \omega^2 u(\Omega_0)w - fw - \alpha H u(\Omega_0)w + 2\alpha^2 u(\Omega_0)w\right)\mathrm{d}\sigma.$$

Now, if we add to the objective function the volume constraint with the Lagrange coefficient η (see (7))

$$J_1(\Omega, u) = J(\Omega, u) + \eta\left(\mathrm{Vol}(\Omega) - \mathrm{Vol}(\Omega_0)\right)^2,$$

the shape derivative of the objective function J_1 is given by

$$J_1'(\Omega_0)(\theta) = J'(\Omega_0)(\theta) + 2\eta\int_{\Gamma_0}\theta\cdot n\left(\mathrm{Vol}(\Omega) - \mathrm{Vol}(\Omega_0)\right)\mathrm{d}\sigma,$$

which concludes the proof of Theorem 1. □

4 Shape optimization algorithm

We want to solve numerically, using the gradient descent method, the following minimization problem: for $\omega > 0$ and Ω_0 given, find $\Omega^{\mathrm{opt}} \in U_{ad}(\lambda, \Omega_0)$, such that

$$J_1(\Omega^{\mathrm{opt}}) = \min_{\Omega\in U_{ad}(\lambda,\Omega_0)} J_1(\Omega).$$

We notice that if the velocity $\mathcal{V}$, defined in Eq. (10), follows the outward normal direction, or equivalently, if $\theta\cdot n = \mathcal{V}$, then Eq. (9) implies that

$$J_1'(\Omega_0)(\theta) = -\int_{\Gamma_0}\mathcal{V}^2\mathrm{d}\sigma < 0,$$

which ensures the decreasing behavior of the objective function. In order to calculate the velocity $\mathcal{V}$, we need to know u, the solution of the Helmholtz equation in Ω_0, but also w, the solution of the adjoint problem and the curvature H. Inspired by [9, 24, 25], we construct a shape optimization algorithm composed of the following steps:

(i) Solving the Helmholtz equation (1) and its adjoint problem 17 by a cell-centered finite difference scheme on a square Cartesian mesh covering Ω.

(ii) Calculating the velocity $\mathcal{V}$ of the Robin boundary Γ, based on formula (10), and then extending this velocity in the direction of the normal vector on the whole domain D, or at least around the Robin boundary.

(iii) Solving the level set equation to obtain a new shape.

If $J_1'(\Omega)(\theta) \geq 0$, then Ω is an optimal domain, and the algorithm stops. In order to describe the shape of the domain, we use a concept of level sets. More precisely, the level set function ψ of the domain $\Omega \subset D$ is defined by

$$\begin{cases} \psi(x) = 0 & \text{iff} \quad x \in (\partial\Omega \cap D), \\ \psi(x) < 0 & \text{iff} \quad x \in \Omega, \\ \psi(x) > 0 & \text{iff} \quad x \in (D \setminus \Omega). \end{cases}$$

The level set method, initially devised by S. Osher and J-A. Sethian in Ref. [24], allows, not only to define implicitly the domain, but also to follow easily the propagation of the boundary during the evolution process. Let us take into account a particle $x(t)$ on the boundary, which propagates in time, hence it has the zero-level set all time, *i.e.*, $\psi(x(t), t) = 0$. By the chain rule, it yields that

$$\psi_t + x'(t) \cdot \nabla\psi\left(x(t), t\right) = 0. \tag{22}$$

If $\mathcal{V}$ is the velocity in the outward normal direction of the boundary, *i.e.* $x'(t) \cdot n = \mathcal{V}$, with $n = \frac{\nabla\psi}{|\nabla\psi|}$, then from Eq. (22), we obtain a so-called level set equation

$$\psi_t + \mathcal{V}|\nabla\psi| = 0, \tag{23}$$

associated with the initial condition $\psi|_{t=0} = \psi_0(x)$, defined by the signed distance function

$$\psi_0(x) = \pm \text{dist}[x, \Gamma], \quad x \in D. \tag{24}$$

In the last formula, Γ is the Robin boundary, and the sign plus (or minus) corresponds to outside (or inside) of the domain Ω. This equation is of Hamilton-Jacobi type, and in what follows we call it the Hamilton-Jacobi equation. Let us notice, that we need to calculate the solution of the Hamilton-Jacobi equation (23) not only in Ω, but in D, and thus, we need to know $\mathcal{V}$ for all $x \in D$. Hence, knowing initially $\mathcal{V}$ only in Ω by formula (10), we need to extend it to all D. More precisely, to calculate numerically $-\mathcal{V}$ on Ω (see Eq. (10)), we first find numerically the solutions u of the Helmholtz problem (1) and w of the adjoint problem (17) and then evaluate ∇u and ∇w. The curvature H is calculated, on the basis of the level set function ψ, by the following equality

$$H = \nabla \cdot \frac{\nabla\psi}{|\nabla\psi|} = \frac{\psi_{yy}\psi_x^2 - 2\psi_x\psi_y\psi_{xy} + \psi_{xx}\psi_y^2}{\left(\psi_x^2 + \psi_y^2\right)^{3/2}}.$$

Once we know $\mathcal{V}$ in Ω, we extend it outside of the domain [26, 25], solving until the stationary state the equation

$$\phi_t + \beta(x, y)\nabla\phi \cdot n = 0,$$

with the initial condition $\phi(t = 0)$ equal to $\mathcal{V}$ inside the domain Ω and zero elsewhere. Here n is defined everywhere in D by $\frac{\nabla\psi}{|\nabla\psi|}$ and β is zero or one corresponding to inside or outside of the domain Ω.

In the aim to penalize too complicated geometries of Γ, the mesh, used to solve the Hamilton-Jacobi equation, is chosen coarser than the mesh used to solve the Helmholtz equation. We use an upwind scheme for solving the Hamilton-Jacobi equation [26, 25] and discretize Eq. (23) as follows

$$\frac{\psi_{ij}^{n+1} - \psi_{ij}^n}{\Delta t} + \left[\max\left(V_{ij}, 0\right)\nabla^+ + \min\left(V_{ij}, 0\right)\nabla^-\right] = 0, \tag{25}$$

where

$$\nabla^+ = \left[\max\left(D_{ij}^{-x},0\right)^2 + \min\left(D_{ij}^{+x},0\right)^2 + \max\left(D_{ij}^{-y},0\right)^2 + \min\left(D_{ij}^{+y},0\right)^2\right]^{1/2},$$
$$\nabla^- = \left[\max\left(D_{ij}^{+x},0\right)^2 + \min\left(D_{ij}^{-x},0\right)^2 + \max\left(D_{ij}^{+y},0\right)^2 + \min\left(D_{ij}^{-y},0\right)^2\right]^{1/2},$$
$$D_{ij}^{-x} = \frac{\psi^n(i,j) - \psi^n(i-1,j)}{\Delta x}, \quad D_{ij}^{+x} = \frac{\psi^n(i+1,j) - \psi^n(i,j)}{\Delta x},$$
$$D_{ij}^{-y} = \frac{\psi^n(i,j) - \psi^n(i,j-1)}{\Delta y}, \quad D_{ij}^{+y} = \frac{\psi^n(i,j+1) - \psi^n(i,j)}{\Delta y},$$

and $\psi|_{t=0} = \psi_0$ is the signed distance function, defined in (24). With a space-step $\Delta x = \Delta y$ scheme (25) is stable under the following CFL condition

$$\Delta t \leq \frac{\Delta x}{\max(|\mathcal{V}(x,y)|)\sqrt{2}}. \tag{26}$$

5 Numerical experiments

For all numerical tests, presented below, we consider the rectangle $\overline{D} = [0,3] \times [0,1]$, and suppose that D always contains the domain Ω, on which we solve the Helmholtz equation. The boundaries Γ_N and Γ_D are fixed and descibed by $\{y = 0, 0 \leq x \leq 2\} \cap \{y = 1, 0 \leq x \leq 2\}$ and $\{x = 0, 0 \leq y \leq 1\}$ respectively, and Γ is the moving boundary inside of $\overline{G} = [\frac{3}{2}, 3] \times [0,1]$. The initial $\Omega_0 =]0,2[\times]0,1[$ has a flat boundary Γ_0 fixed at $x = 2$. The characteristic lengths of Ω_0 are $\ell = 1$ and $L = 2\ell$.

The Helmholtz equation is considered with a wave number $k = \frac{\omega}{c_0}$, *i.e*,

$$\Delta u + k^2 u = -f,$$

where c_0 is the sound speed in air. We take

$$f = 0, \quad g = \frac{1}{\sigma\sqrt{2\pi}} \exp\left(-\frac{(y-1/2)^2}{2\sigma^2}\right)$$

with $\sigma = 1$ in the Helmholtz boundary value problem. For the chosen σ, the smallest wavelength, excited by g, is $\lambda = \frac{\ell}{2}$. The parameter α in the Robin boundary condition depends on the value of the frequency ω. It is calculated for ISOREL, using a minimization of the difference between the solution of the problem with a volume dissipation (described by a damped wave equation) and the solution of the problem with the boundary dissipation for the flat shape of Γ (see Theorem B.1 [1]). We solve the Helmholtz boundary value problem on a fine mesh with the size $h = \frac{\ell}{64}$. For waves with the wavelength equal to $\frac{\ell}{2}$, this typically gives dispersion errors of the order 10^{-3}, since the dispersion error due to the centered finite difference approximation of the Laplacian is known to be $\frac{(kh)^2}{24}$, with $kh = \frac{2\pi}{32}$ here. We perform the level set approach for the optimization algorithm on the coarse mesh of the size $\kappa = 2h = \frac{\ell}{32}$ (in the aim of a penalization of too much complicated shapes of Γ). However, we notice that $\kappa \ll \lambda$.

5.1 Properties of the optimization algorithm

Let us illustrate the stability properties of the optimization algorithm.

We fix the frequency $\omega_0 = 3170$, which is a local maximum of

$$J(\Omega)(\omega) = \int_\Omega |u|^2 \mathrm{d}x,$$

calculated for $\Omega_0 =]0,2[\times]0,1[$ in a range of frequencies, for instance, $\omega \in [3000, 6000]$. This time we chose $A = 1$ and $B = C = 0$ for the simulation of the acoustical energy.

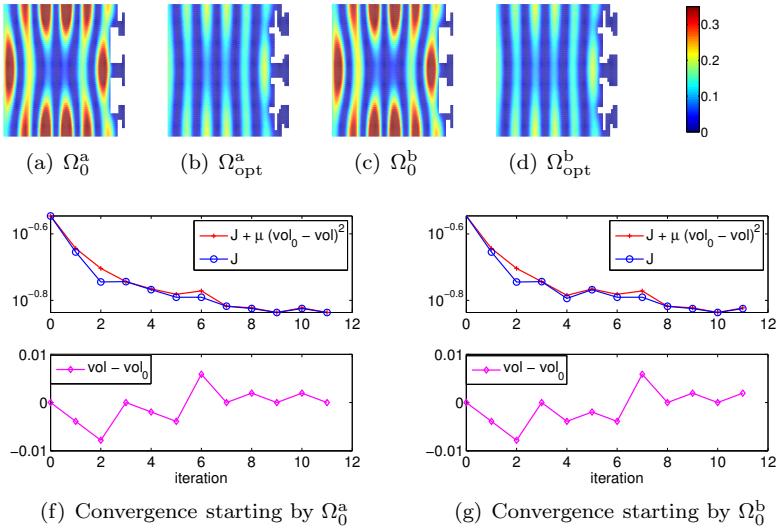

(a) Ω_0^{a} (b) $\Omega_{\mathrm{opt}}^{\mathrm{a}}$ (c) Ω_0^{b} (d) $\Omega_{\mathrm{opt}}^{\mathrm{b}}$

(f) Convergence starting by Ω_0^{a} (g) Convergence starting by Ω_0^{b}

Figure 1: The values of $|u|^2$ are presented on two initial and optimal domains for the fixed frequency $\omega_0 = 3170$. From left to right: the initial domain Ω_0^a and the corresponding optimal domain $\Omega_{\mathrm{opt}}^a = \Omega_{11}^a$, the initial domain Ω_0^b, taken in a small neighborhood of Ω_0^a, and the corresponding optimal domain $\Omega_{\mathrm{opt}}^b = \Omega_{10}^b$. We see that Ω_{opt}^a is in a small neighborhood of Ω_{opt}^b (the shapes of Γ^a and Γ^b are almost the same). The values of J are also almost the same: $J(\Omega_{\mathrm{opt}}^a)(\omega_0) \approx 0.1458$ and $J(\Omega_{\mathrm{opt}}^b)(\omega_0) \approx 0.1458$. As compared to the flat shape $\overline{\Omega}_0 = [0,2] \times [0,1]$, for which $J(\Omega_0)(\omega_0) = 4.286$, we have $J(\Omega_0)(\omega_0)/J(\Omega_{\mathrm{opt}}^a)(\omega_0) = 27.492$, hence the optimal shapes dissipate the energy 27.5 times better than the flat one. The bottom pictures show the convergence of the optimization algorithm for two cases of initial domain: for Ω_0^a in the left and for Ω_0^b in the right.

If we start the optimization algorithm one time from $\Omega_0 = \Omega_0^a$ and the second time from $\Omega_0 = \Omega_0^b$, such that the Hausdorff distance $d_H(\Omega_0^a, \Omega_0^b) < \varepsilon$ is small enough, then the optimal shapes Ω_{opt}^a and Ω_{opt}^b are "almost the same", *i.e.* there exists $C > 0$, depending only on ε, such that the Hausdorff distance

$$d_H(\Omega_{\mathrm{opt}}^a, \Omega_{\mathrm{opt}}^b) < C(\varepsilon) d_H(\Omega_0^a, \Omega_0^b)$$

is also small. Hence, $|J(\Omega_{\mathrm{opt}}^a)(\omega_0) - J(\Omega_{\mathrm{opt}}^b)(\omega_0)| \ll 1$ is also small by the continuity of J as a function of the domain; see Fig. 1 for a numerical example.

Let us also notice, that, as for the question of Mark Kac "Can one hear the shape of a drum?" [17, 19, 18], we don't have the uniqueness of the optimal shape Γ, since different shapes can have the same spectrum and be identically efficient in the dissipation of the energy in the fixed range of frequency. Fig. 2 illustrates the case, when the initial shape $\Omega_0 = \Omega_0^c$ is not in a small neighborhood of Ω_{opt}^a and the characteristic geometric scales of Ω_0^c are almost the same as for Ω_{opt}^a. For this choice of Ω_0^c we obtain that Ω_{opt}^c is not in a small neighborhood of $\Omega_{\mathrm{opt}}^{\mathrm{flat}}$, but we still have $|J(\Omega_{\mathrm{opt}}^c)(\omega_0) - J(\Omega_{\mathrm{opt}}^a)(\omega_0)| \ll 1$. Moreover, Fig. 3 shows, that the values of the functional $|J(\Omega_{\mathrm{opt}}^c)(\omega) - J(\Omega_{\mathrm{opt}}^a)(\omega)| \ll 1$ are almost the same for all ω in a rather large neighborhood of ω_0.

Fig. 3 also shows that the minimization process for one given frequency (here $\omega_0 = 3170$, corresponding to the middle peak of $J(\Omega^{\mathrm{flat}})$) is very efficient, but it creates as expected peaks at other frequencies, and so, we need a strategy to find the most efficient shape, able to dissipate the acoustical energy in a large range of frequencies.

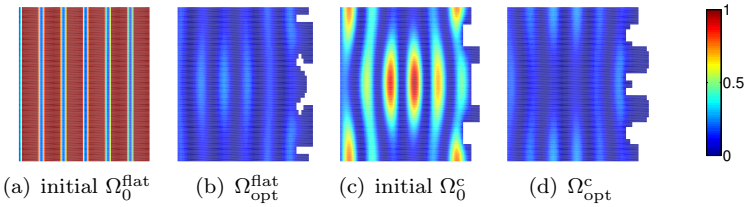

(a) initial Ω_0^{flat} (b) $\Omega_{\text{opt}}^{\text{flat}}$ (c) initial Ω_0^{c} (d) $\Omega_{\text{opt}}^{\text{c}}$

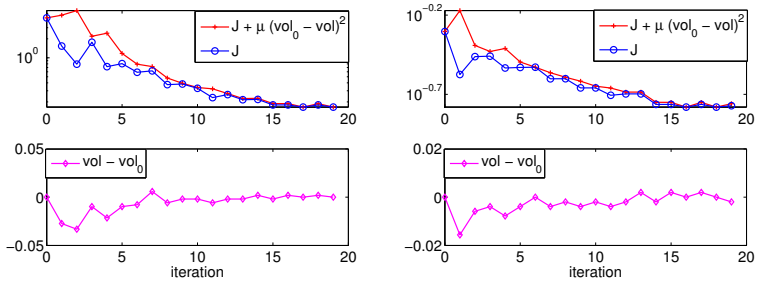

(f) Convergence starting by Ω_0^{flat} (g) Convergence starting by Ω_0^{c}

Figure 2: The values of $|u|^2$ are presented on two initial and optimal domains for the fixed frequency $\omega_0 = 3170$. From left to right: the initial domain Ω_0^{flat} and the corresponding optimal domain $\Omega_{\text{opt}}^{\text{flat}}$, the initial domain Ω_0^{c}, significantly different to Ω_0^{flat} and to $\Omega_{\text{opt}}^{\text{flat}}$, taken with characteristic geometric scales which are almost the same as for $\Omega_{\text{opt}}^{\text{flat}}$, and the corresponding optimal domain $\Omega_{\text{opt}}^{\text{c}}$. We see that $\Omega_{\text{opt}}^{\text{flat}}$ is not in a small neighborhood of $\Omega_{\text{opt}}^{\text{c}}$ (the shapes of Γ^a and Γ^b are really different). But the values of J for $\omega_0 = 3170$ are also almost the same: $J(\Omega_{\text{opt}}^{\text{flat}}) = 0.1654$ and $J(\Omega_{\text{opt}}^{\text{c}}) = 0.1659$.

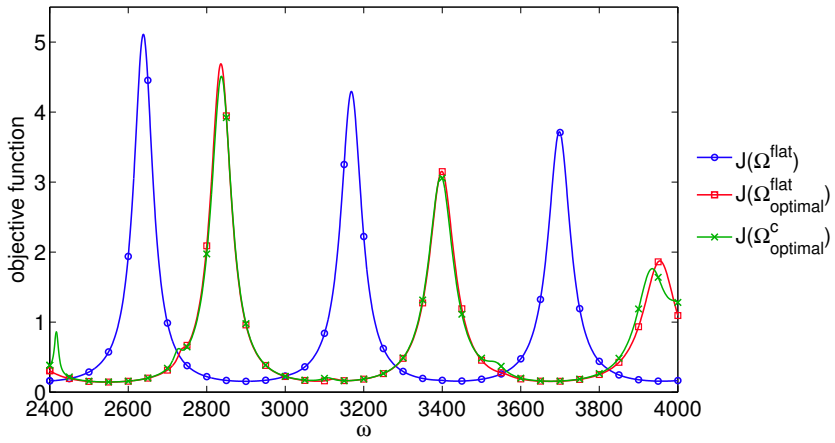

Figure 3: The objective function J as a function of ω for the flat shape Ω_0, for the optimal shape $\Omega_{\text{opt}}^{\text{flat}}$ (see Fig. 2) and for the optimal shape $\Omega_{\text{opt}}^{\text{c}}$ (see Fig. 2).

5.2 Optimized "simple" wall for a large range of frequencies

In this subsection, we are searching a shape of the wall Ω, which could be as absorbing as possible in terms of the acoustic energy $J(\Omega)(\omega) = \int_\Omega |u|^2 \mathrm{d}x$ in a large range of frequencies with the simplest possible design. Let us fix the range of frequencies for the energy

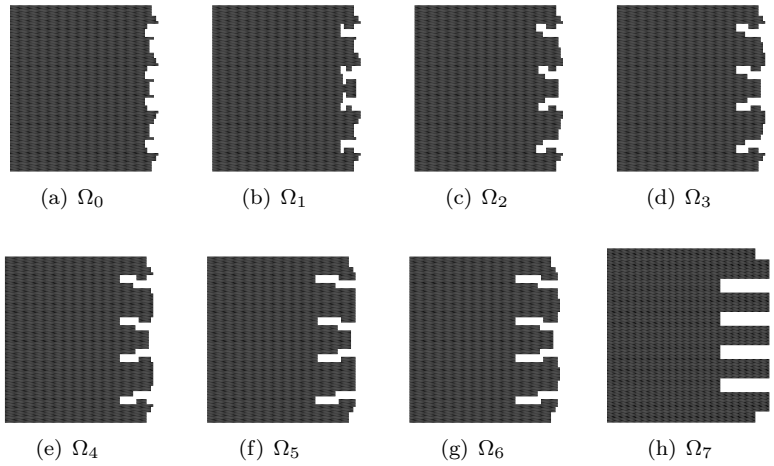

(a) Ω_0 (b) Ω_1 (c) Ω_2 (d) Ω_3

(e) Ω_4 (f) Ω_5 (g) Ω_6 (h) Ω_7

Figure 4: Shapes, which are used in the optimization algorithm process: from left to right in the top line- Ω_0 (the initial shape), Ω_k, $k = 1, 2, 3$, and from left to right in the bottom line - Ω_k, $k = 4, 5, 6, 7$. The domain Ω_7 is generated manually in the aim to simplify the final shape Ω_6.

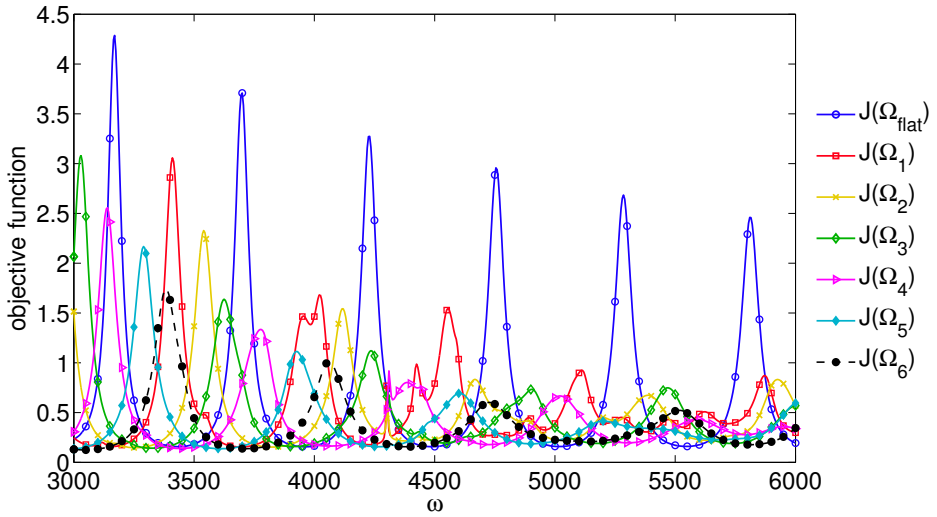

Figure 5: The values of the objective function $J(\Omega_0)$ $(A = 1, B = 0, C = 0)$ for the flat shape as a function of $\omega \in [3000, 6000]$ are presented by the line with circles, the values of $J(\Omega_1)$ (see Fig. 4 for the shape of Ω_1) are presented by the line with squares, the values of $J(\Omega_2)$ by the line with stars, those of $J(\Omega_3)$ by the line with empty rhombus, those of $J(\Omega_4)$ by the line with arrows, those of $J(\Omega_5)$ by the line with full rhombus, and those of $J(\Omega_6)$ by the black dash-dotted line.

dissipation: $\omega \in [3000, 6000]$.

As in 5.1, we fix the frequency $\omega_0 = 3170$ of a local maximum of J on $\Omega_{\text{flat}} =]0, 2[\times]0, 1[$. We perform the shape optimization algorithm for this frequency, taking as the initial shape Ω_0, given on Fig. 4, and we obtain Ω_1, optimal at $\omega = 3170$. Noticing that all local maxima of $J(\Omega_1)$ are smaller than the local maxima of $J(\Omega_{\text{flat}})$ (see Fig. 5), we choose Ω_1 as the initial domain and restart the optimization algorithm, minimizing in the neighborhood of

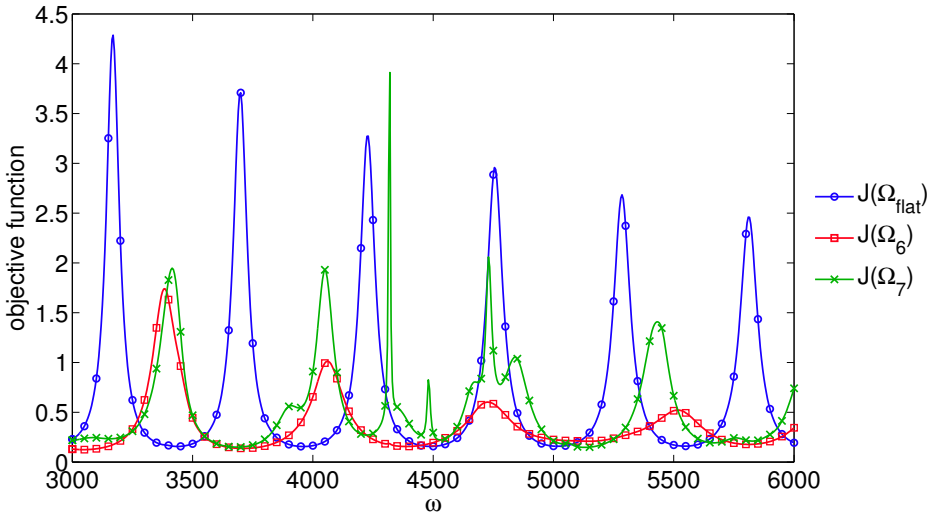

Figure 6: Comparison of the dissipative properties of the flat shape Ω_{flat}, the optimal Ω_6 and of its simplification Ω_7. The values of $J(\Omega_{\text{flat}})$, of $J(\Omega_6)$ and of $J(\Omega_7)$ $(A = 1, B = 0, C = 0)$ as functions of $\omega \in [3000, 6000]$ are given by the lines with circles, squares and stars respectively.

Ω_1 the sum of functionals $\sum_{k=1}^{3} J(\Omega)(\omega_k)$, where $\omega_1 = 3410$, $\omega_2 = 4025$ and $\omega_3 = 4555$ are the local maxima of $J(\Omega_1)$. This minimization gives the optimal shape Ω_2, such that

1. Ω_2 is almost optimal in the neighborhood of ω_k for $k = 0, 1, 2, 3$;
2. all local maxima of $J(\Omega_2)$ are smaller than the local maxima of $J(\Omega_1)$.

Choosing $\omega_4 = 3625$ and $\omega_5 = 4240$, corresponding to the local maxima of $J(\Omega_2)$, we take Ω_2 as the initial domain and restart the optimization algorithm, minimizing $J(\Omega)(\omega_4)+J(\Omega)(\omega_5)$ to obtain the optimal shape Ω_3, such that

1. Ω_3 is almost optimal in the neighborhood of ω_k for $k = 0, \ldots, 5$;
2. all local maxima of $J(\Omega_3)$ are smaller than the local maxima of $J(\Omega_2)$.

We iterate this process up to Ω_6 and we are stopped by the restriction that Γ must be contained in the area $\overline{G} = [\frac{3}{2}, 3] \times [0, 1]$.

The shape of Ω_6 contains multiscale details, which ensures the dissipative performances of the wall in a large range of frequencies (see Fig. 5). Thinking about the demolding process of wall construction, we simplify the geometry of Ω_6, deleting the multi-scales and keeping only the largest characteristic scale of Ω_6 (see the domain Ω_7, generated by hand, on Fig. 4). As we can see from Fig. 6, since we have kept almost unchanged the largest characteristic geometric size for Ω_6 and Ω_7, the energy dissipation is also almost the same in the corresponding range of frequencies (see red and green lines for $[3000, 3700]$ on Fig. 6). As all smaller scale details have been deleted, the shape of Ω_7 is not as good as the shape of Ω_6 to dissipate higher frequencies (see lines with squares and stars for $[3700, 6000]$ on Fig. 6). Hence, Fig. 6 shows that the compromises between two desired properties "to be the most dissipative" (as Ω_6 here) and "to be simple to construct" (on the example of Ω_7) is not too bad, especially if we know the most important frequencies to dissipate.

Fig. 7–Fig. 9 show the energy distribution for three values of frequencies illustrating the three typical cases: $J(\Omega_6) \approx J(\Omega_7)$, $J(\Omega_6) < J(\Omega_7)$ and $J(\Omega_7)$ has its local maximum (see Fig. 6).

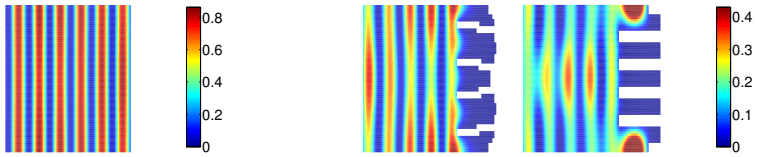

(a) $|u(\Omega_{\text{flat}})|^2$ (c) $|u(\Omega_6)|^2$ (d) $|u(\Omega_7)|^2$

Figure 7: Energy distribution in Ω_{flat}, Ω_6 and Ω_7 respectively for $\omega = 3235$, corresponding to the case when $J(\Omega_6) \approx J(\Omega_7)$ are almost the same (precisely $J(\Omega_6) = 0.2841$, $J(\Omega_7) = 0.2829$)

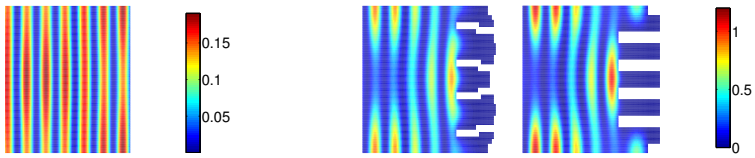

(a) $|u(\Omega_{\text{flat}})|^2$ (c) $|u(\Omega_6)|^2$ (d) $|u(\Omega_7)|^2$

Figure 8: Energy distribution in Ω_{flat}, Ω_6 and Ω_7 respectively for $\omega = 3495$, corresponding to the case when $J(\Omega_6) = 0.4767$ and $J(\Omega_7) = 0.5077$ take slight different values.

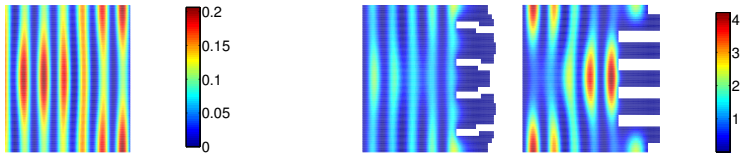

(a) $|u(\Omega_{\text{flat}})|^2$ (c) $|u(\Omega_6)|^2$ (d) $|u(\Omega_7)|^2$

Figure 9: Energy distribution in Ω_{flat}, Ω_6 and Ω_7 respectively for $\omega = 3415$, the frequency which yields a local maximum of the objective function on the domain Ω_7.

References

[1] F. Magoulès, T. P. K. Nguyen, P. Omnès, and A. Rozanova Pierrat. Optimal absorption of acoustical waves by a boundary. *Submitted*, 2020.

[2] S. Félix, M. Asch, M. Filoche, and B. Sapoval. Localization and increased damping in irregular acoustic cavities. *Journal of Sound and Vibration*, 299(4-5):965–976, Feb 2007.

[3] D. Duhamel. *Calcul de murs antibruit et control actif du son.* PhD thesis, Mémoire dhabilitation, 1998.

[4] D. Duhamel. Shape optimization of noise barriers using genetic algorithms. *Journal of Sound and Vibration*, 297(1-2):432–443, Oct 2006.

[5] D. Guicking. On the invention of active noise control by Paul Lueg. *The Journal of the Acoustical Society of America*, 87(5):2251, 1990.

[6] K. Abe, T. Fujiu, and K. Koro. A BE-based shape optimization method enhanced by topological derivative for sound scattering problems. *Engineering Analysis with Boundary Elements*, 34(12):1082–1091, Dec 2010.

[7] Y. Cao and D. Stanescu. Shape optimization for noise radiation problems. *Computers & Mathematics with Applications*, 44(12):1527–1537, Dec 2002.

[8] B. Farhadinia. An Optimal Shape Design Problem for Fan Noise Reduction. *JSEA*, 03(06):610–613, 2010.

[9] G. Allaire. *Conception optimale de structures.* 58 Mathématiques et Applications, Springer, 2007.

[10] B. Mohammadi and O. Pironneau. *Applied shape optimization for fluids.* Oxford University Press, 2010.

[11] Y. Achdou and O. Pironneau. Optimization of a photocell. *Optimal Control Applications and Methods*, 12(4):221–246, Oct 1991.

[12] A. Münch. Optimal Internal Dissipation of a Damped Wave Equation Using a Topological Approach. *International Journal of Applied Mathematics and Computer Science*, 19(1), Jan 2009.

[13] A. Münch, P. Pedregal, and F. Periago. Optimal design of the damping set for the stabilization of the wave equation. *Journal of Differential Equations*, 231(1):331–358, Dec 2006.

[14] S. Cox and E. Zuazua. The rate at which energy decays in a damped string. *Communications in Partial Differential Equations*, 19(1-2):213–243, Jan 1994.

[15] M. Asch and G. Lebeau. The Spectrum of the Damped Wave Operator for a Bounded Domain in $\mathbb{R}^2$. *Experimental Mathematics*, 12(2):227–241, Jan 2003.

[16] H. Antil, S. Hardesty, and M. Heinkenschloss. Shape Optimization of Shell Structure Acoustics. *SIAM Journal on Control and Optimization*, 55(3):1347–1376, Jan 2017.

[17] A. Girouard, L. Parnovski, I. Polterovich, and D. A. Sher. The Steklov spectrum of surfaces: asymptotics and invariants. *Mathematical Proceedings of the Cambridge Philosophical Society*, 157(03):379–389, Aug 2014.

[18] C. Gordon, P. Perry, and D. Schueth. Isospectral and isoscattering manifolds: a survey of techniques and examples. *Geometry, spectral theory, groups, and dynamics, Contemp. Math.*, 387:157–179, 2005.

[19] C. Gordon, P. Herbrich, and D. Webb. Robin and Steklov isospectral manifolds. *preprint*, 2015.

[20] M. J. Gander, L. Halpern, and F. Magoulès. An optimized Schwarz method with two-sided Robin transmission conditions for the Helmholtz equation. *International Journal for Numerical Methods in Fluids*, 55(2):163–175, 2007.

[21] S. Agmon. *Lectures on elliptic boundary value problems.* Van Mostrand Math. Studies, 1965.

[22] D. Chenais. On the existence of a solution in a domain identification problem. *Journal of Mathematical Analysis and Applications*, 52(2):189–219, Nov 1975.

[23] A. Henrot and M. Pierre. *Variation et optimization de formes. Une analyse géométrique.* Springer, 2005.

[24] S. Osher and J.-A. Sethian. Fronts propagating with curvature dependent speed: algorithm based on Hamilton-Jacobi formulations. *J. Comp. Phys*, 79, 1988.

[25] J. Sethian and R. Fedkiw. *Level set method and fast marching methods.* Cambridge Univerity Press, 1999.

[26] S. Osher and R. Fedkiw. *Level set method and dynamic implicit surfaces*, volume 153. Applied Mathematical Sciences, Springer, 2003.